InAs nanowire superconducting tunnel junctions: Quasi-particle spectroscopy, thermometry, and nanorefrigeration

Jaakko Mastomäki[1,2], Stefano Roddaro[1,*], Mirko Rocci[1], Valentina Zannier[1], Daniele Ercolani[1], Lucia Sorba[1], Ilari J. Maasilta[2], Nadia Ligato[1], Antonio Fornieri[1], Elia Strambini[1], and Francesco Giazotto[1,*]

[1] NEST, Scuola Normale Superiore and Istituto Nanoscienze-CNR, Piazza S. Silvestro 12, I-56127 Pisa, Italy

[2] Nanoscience Center, Department of Physics, University of Jyvaskyla, 40014 Jyväskylä, Finland

[*] stefano.roddaro@sns.it, francesco.giazotto@sns.it

ABSTRACT

We demonstrate an original method based on controlled oxidation for creating high-quality tunnel junctions between superconducting Al reservoirs and InAs semiconductor nanowires (NWs). We show clean tunnel characteristics with a current suppression by >4 orders of magnitude for a junction bias well below the Al gap of $\Delta_0 \approx 200$ μeV. The experimental data agree well with the Bardeen–Cooper–Schrieffer theoretical expectations for a superconducting tunnel junction. The studied devices employ small-scale tunnel contacts functioning as thermometers as well as larger electrodes that provide proof-of-principle active cooling of the electron distribution in the NWs. A peak refrigeration of approximately $\delta T = 10$ mK is achieved at a bath temperature of $T_{bath} \approx 250$–350 mK for our prototype devices. This method introduces important perspectives for the investigation of the thermoelectric effects in semiconductor nanostructures and for nanoscale refrigeration.

KEYWORDS

InAs nanowire, superconducting tunnel junction, thermometry, nanorefrigeration

1 Introduction

Control of the heat flow and the local electron distribution in nanodevices is a crucial experimental challenge [1–3] with an important impact on both the solution of key open problems in fundamental physics and the development of future device applications [4, 5]. In particular, the recent progress of thermoelectric physics in nanostructured materials offers fascinating new perspectives for the realization of more efficient solid-state heat pumps for energy conversion [6–8] and/or for the creation of self-cooling nanodevices where the electron or the phonon system in the active region can be refrigerated below the phonon bath [3–4]. The progress in these fields calls for the development of novel methods to reliably control heat and measure the device thermoelectric parameters with nanometer-scale precision [9–12]. Local electronic cooling can be relevant for improving the device performance in terms of noise, sensitivity, or decoherence [4] and for finding a role in advanced applications, including topological quantum computation [13–16] and ultrasensitive radiation detection [17, 18]. In addition, the manipulation of heat is the basis of the emerging field of coherent caloritronics [1, 19–21] and can be crucial for solving important standing fundamental problems in condensed-matter physics, including quantum thermodynamics and the study of the elusive Majorana fermions in solid-state systems [13, 22, 23].

Hybrid architectures combining superconductive elements with normal metals represent a promising example of a refined technology for locally measuring and manipulating heat at low temperatures and have been the subject of extensive research efforts [3–5]. In particular, devices integrating normal-insulator-superconductor (NIS) tunnel junctions between a normal metal (N) and Al [24] or other superconductors (S) [25, 26] have exhibited significant nanorefrigeration in the milliKelvin regime. Thus far, a similar technology has been difficult to achieve in the context of semiconductor nanostructures, given the notorious technical challenges that the realization of clean semiconductor interfaces entails [27]. While alternative approaches exist [28], they cannot offer a comparable performance, especially with regard to the

cooling power [24]. In this study, we combined superconductive tunnel contacts with the technology of self-assembled semiconductor nanowires (NWs). NW technology has recently been used to create advanced nanodevices in the context of thermoelectrics [7], Josephson devices [29, 30], single-electron manipulation [31–34], topological quantum computing, and Majorana physics [13–16], but none of these applications utilized hard tunnel junctions. In this study, we exploit the controlled oxidation of a thin layer of an Al alloy to fabricate junctions with a controlled transparency and use InAs NWs to create SI(NW)IS tunnel devices. We demonstrate that this technique can be used to obtain state-of-the-art tunnel characteristics, which can be exploited to perform sensitive local thermometry using nanoscale contacts. In addition, large junctions are used to demonstrate the electron cooling of an individual NW: A peak refrigeration of δT = 10 mK is demonstrated in the current device architecture, which is expected to be significantly improved with a better device geometry.

Devices were built starting from degenerately Se-doped *n*-type InAs NWs [35] grown via chemical beam epitaxy (Methods). The wires were deposited on a SiO_2/Si substrate via dropcasting and placed in contact with metal electrodes fabricated via electron-beam lithography. The SiO_2 layer was 300 nm thick and provided good isolation between the device and the Si substrate. Four electrodes were fabricated on each NW, as shown in Fig. 1(a), with two small-scale, 200-nm-wide fingers at the central part of the nanostructure and two larger contacts at the two ends of the NW. The central electrodes were designed to function as tunnel thermometers and were separated by approximately 300 nm. The outer tunnel electrodes had large junction areas (approximately 90 nm × 600 nm) and were designed to control the electron distribution in the NWs. Their nominal separation from the inner electrodes was also 300 nm. A simplified sketch of the setup used to measure the electronic temperature and to refrigerate the electrons in the NWs is shown in Fig. 1(b). The key details of the contact technology discussed here are illustrated in Fig. 1(c). Tunnel contacts were obtained by multiple steps of electron-beam lithography, evaporation, and controlled *in situ* oxidation. After the electron-beam patterning and development, the InAs surface was passivated by using a $(NH_4)_2S_x$ solution [36] to remove the native oxide. The sample was then immediately transferred to the vacuum chamber of an electron-beam evaporator, where a 5/50 nm-thick layer of Ti/AlMn was evaporated. The purpose of the Mn impurities in the alloy was to quench the superconductivity in the Al-based

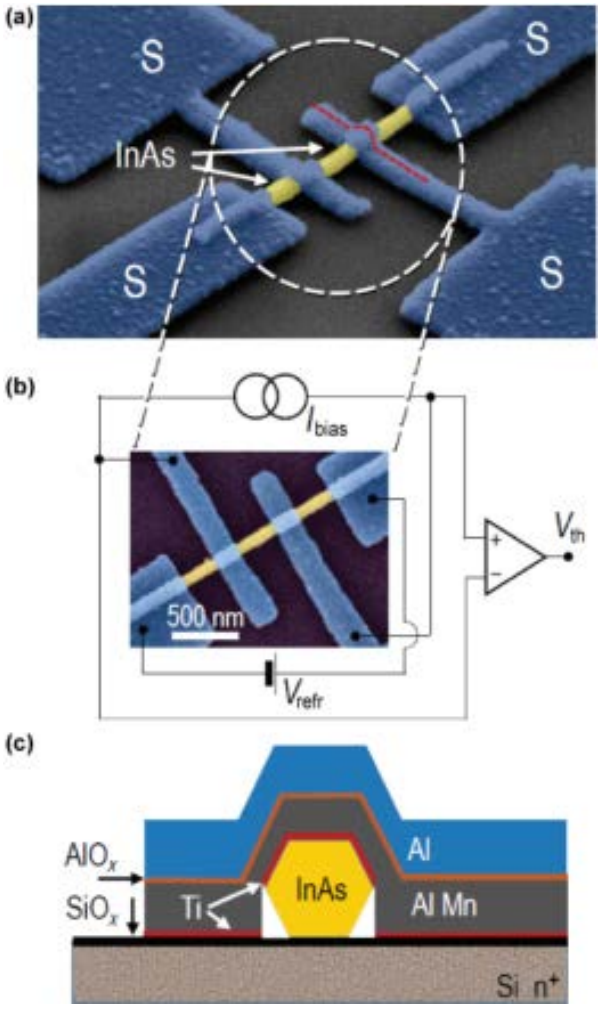

Figure 1 Device architecture. (a) Scanning electron micrograph of a typical device: Four tunnel junctions were created between the superconductive electrodes (S) and an *n*-doped InAs NW. Two 200-nm-wide inner contacts were used to measure the electron temperature in the InAs nanostructure. Two larger contacts were fabricated at the two ends of the NW and were used to extract hot carriers from the InAs and to refrigerate its electron system below the bath temperature. The sample was imaged at an angle of 50°. (b) Local thermometry was achieved by biasing the inner contacts with a constant current of I_{bias} and by measuring the resulting voltage drop V_{th} in the four-wire scheme; refrigeration was achieved by biasing the outer contact with a voltage of V_{refr}. (c) Cross-sectional view of the tunnel junction along the dashed red line in (a): the NIS barrier was obtained via the controlled *in situ* oxidation of a 50-nm-thick non-superconductive Al layer containing Mn impurities. A conventional 50-nm-thick superconductive Al layer was evaporated on top of the oxide barrier. A thin 5-nm layer of Ti was deposited between the NW and the AlMN film to promote adhesion.

layer [37], so that it could be used to create a thin normal-metal interlayer between the oxide barrier on top of it and the InAs crystal. In the current architecture, a residual superconductive effect was expected because of the Ti layer. After the first evaporation, the sample was transferred to an oxidation chamber, where the AlMn layer

was exposed to 0.2–0.4 Torr of O_2 for 5 min, which was expected to yield a 1–2-nm-thick oxide layer. Importantly, Mn impurities have no detrimental effects on the barrier quality [37]. After the oxidation, a residual AlMn layer with a thickness of approximately 50 nm remained as a buffer between the oxide and the InAs. In principle, its thickness could be reduced by evaporating a thinner AlMn layer but at the risk of non-homogeneity and thus a lower-quality oxide barrier. Finally, a 50-nm-thick layer of superconductive Al was added on top of the AlO_x.

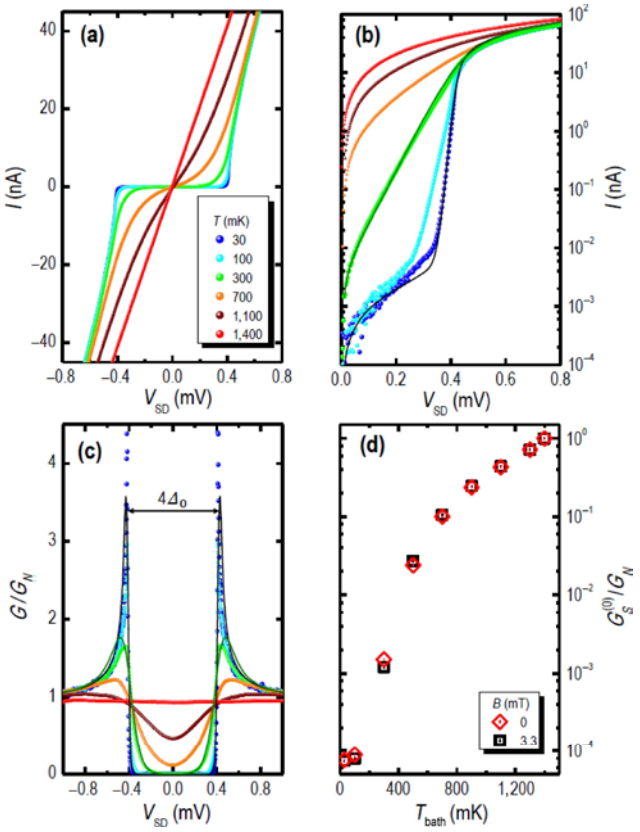

Figure 2 Tunnel conductance and quasiparticle spectrum**.** (a) Selected *IV* curves for a typical SI(NW)IS configuration involving the inner device contacts, under a weak out-of-plane magnetic field of 3.3 mT. (b) Same curves in a semi-log scale. At zero bias, the current I was strongly quenched by the superconductive gap in the Al contacts, indicating high-quality tunnel junctions. Selected experimental data (dots) are compared to BCS theory (solid lines), exhibiting good agreement. (c) As expected for a well-behaved tunnel junction, the differential conductance $G = dI/dV$ was proportional to the convolution of the density of states on the N and S sides of the junctions and the derivative of the Fermi–Dirac distribution. A gap of $\Delta_0 \approx 208$ μeV was determined according to a theoretical fit of the experimental data using BCS theory. The gap can also be estimated according to the distance between the two singularities in the differential conductance if the SI(NW)IS device corresponds to $4\Delta_0$. (d) Normalized zero-bias conductance vs. the bath temperature.

Contacts obtained using the aforementioned procedure typically yielded a low-temperature normal-state resistance of approximately 6.5 and 2.5 kΩ for the small- and large-area NIS barriers, respectively. The NWs typically exhibited an additional ~2 kΩ resistance between the two outer contacts. These resistances were determined separately for each contact and the NW, by measuring every pair combination. The contacts exhibited almost ideal current–voltage (*IV*) characteristics, as shown in Fig. 2, if operated in a small out-of-plane magnetic field of $B = 3.3$ mT. Under these experimental conditions, the *IV* characteristics were consistent with what is expected for a SINIS device; in our case, the N portion of the device was implemented by the InAs NW, in addition to two thin and strongly coupled AlMn interlayers. The temperature evolution of the *IV* curves is shown in Fig. 2(a), indicating the high quality of the tunnel junctions. In the semilog plot of Fig. 2(b), a suppression of approximately 4 orders of magnitude with respect to the normal state was observed in the current at the base temperature of $T_{bath} = 30$ mK when the bias V_{SD} was smaller than the superconductive gap Δ_0. The quality of the tunnel junction can be even better appreciated from the normalized differential conductance G/G_N plot of Fig. 2(c), where $G = dI/dV$, and G_N is the normal-state conductance evaluated at high bias voltages ($V_{SD} >> \Delta_0$) and low temperatures. The *IV* characteristics allow tunnel spectroscopy of the superconductor states, in the sense that they are directly related to the quasiparticle spectrum as a function of the energy (see Eq. (1) in Methods) [38]. The experimental results (dots) shown in Figs. 2(b) and 2(c) were directly compared with Bardeen–Cooper–Schrieffer (BCS) predictions (continuous lines), and a good agreement was obtained assuming $\Delta_0 = 208 \pm 1$ μeV, $R_N = 9.4$ kΩ, and a Dynes parameter of $\gamma = 8 \times 10^{-5}$ (see fit Eq. (2) in Methods). The best fits for the data measured at bath temperatures of 30 and 300 mK were obtained by setting the electron temperatures as 53 and 275 mK, respectively. Figure 2(d) shows the corresponding suppression of the differential conductance with zero magnetic field and with a small off-plane B of 3.3 mT. The field had a marginal effect on the zero-voltage conductance but was important for suppressing extra features in the *IV*, which were likely caused by the residual pairing effects discussed in the next paragraph.

Figure 3 shows the detailed evolution of the tunnel characteristics with respect to the out-of-plane magnetic field B. The *IV* curves and the corresponding normalized differential conductance G/G_N are shown in Figs. 3(a)

and 3(b), respectively. The junction exhibits a complex behavior at zero field, with additional structures in *G*: The effect indicates a residual superconductive gap on the NW side of the tunnel junction, which was likely due to the presence of the Ti layer. The *IV* anomalies were easily quenched by the application of a few-milliTesla magnetic field. The full evolution of the normalized conductance with respect to *B* is illustrated by the colorplot of Fig. 3(c), indicating the expected quenching of the superconductivity in the Al electrodes. The impact ofthe zero-field anomaly visible in Figs. 3(a) and 3(b) can also be easily identified in the colorplot at B < 3 mT. The

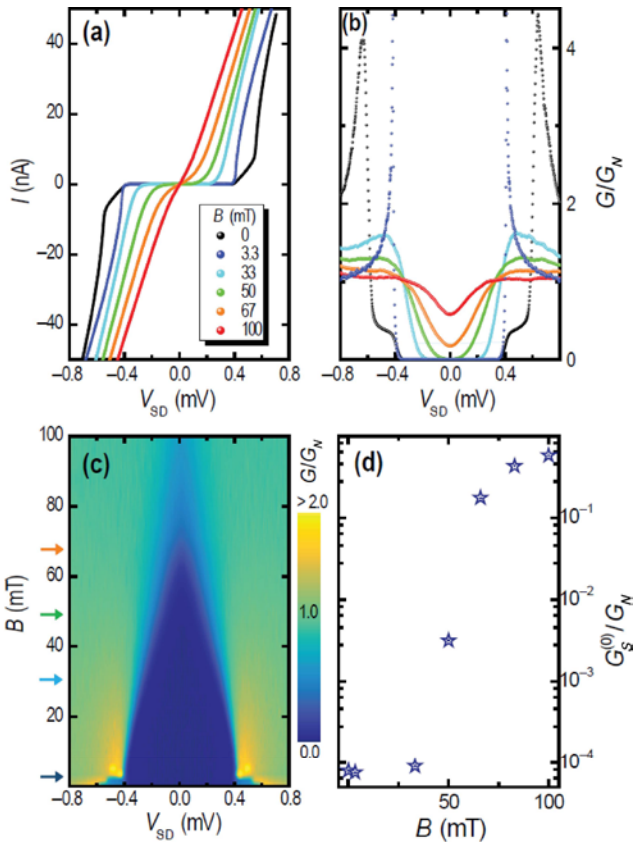

Figure 3 Magnetic-field suppression**.** The junctions exhibit a non-trivial behavior with respect to the magnetic field *B*, as indicated by the *IV* curves in (a) and the corresponding differential conductance traces in (b). In particular, the normalized differential conductance at $B = 0$ indicates a double step in the density of states. The possible origin of this phenomenon is a residual pairing on the NW side of the tunnel junctions (see text). The full evolution of the effect is more clearly observed in (c), which shows the conductance colorplot vs. *B*. A small magnetic field (~3 mT) quenched the residual proximity in the NW. The rest of the evolution is attributed to the quenching of the superconductivity in the Al electrodes, which is also indicated by the evolution of the zero-bias conductance in (b). The arrows in (c) indicate the intermediate values of the magnetic field for the plots in (a) and (b). (d) Evolution of the normalized zero-bias differential conductance with respect to *B*, indicating a critical field of Al of approximately 100 mT.

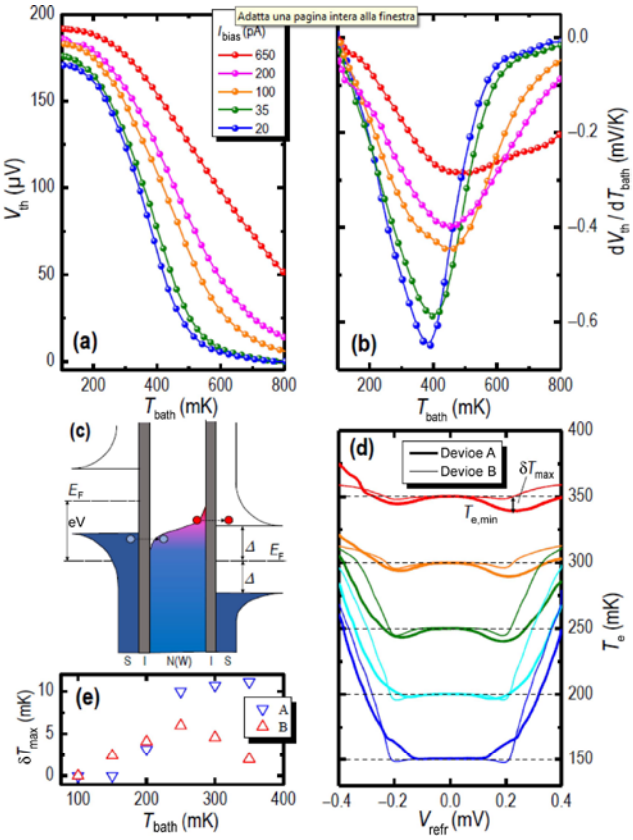

Figure 4 Thermometry and cooling. The inner SI(NW)IS junctions function as a sensitive electronic thermometer, as indicated by the V_{th} voltage response at the fixed current bias I_{bias} in (a). The thermometer response is more clearly shown by the dV_{th}/dT_{bath} plot in (b), indicating a maximum responsivity of over 0.6 mV/K. The outer and larger SI(NW)IS junction was used to tailor the electron distribution in the NW: As shown in (c), a suitable biasing configuration allowed hot carriers to be removed from the central region of the device, reducing its thermal energy [4]. The plot in (d) shows the reduction of the electron temperature T_e with respect to the refrigerator bias V_{refr}, which was measured while biasing the thermometer junctions with $I_{bias} = 20$ pA. Data from two different NW refrigerators (A and B) are shown as thick and thin lines, respectively. A dashed horizontal line indicates the bath temperature T_{bath} corresponding to T_e at zero bias. A top cooling of ~10 mK was achieved starting from $T_{bath} \approx 250$–350 mK, as indicated by the temperature data extracted in (e).

colorplot indicates a critical field of $B_c \gtrsim 100$ mT, which is also observed in the conductance plot $G(B)$ in Fig. 3(d).

Superconducting tunnel contacts can be used for measuring the electronic temperature and for actively cooling the electron distribution in the NW [4]. The narrower inner contacts have a larger barrier resistance and are more suitable for local probing of the temperature. In fact, when thermal energy is small with respect to the superconductive gap, the current in the SI(NW)IS device only depends on the electronic temperature T_e in the NW region, and the tunnel junctions can be used as a thermometer (see Methods). In this case, the probe is gener-

ally operated at a constant bias current I_{bias}, and the corresponding voltage drop V_{th} is a function of only the electronic temperature T_e. A calibration measurement was performed against the refrigerator RuO_2 thermometer in a thermalized regime, that is, $T_e = T_{bath}$. The thermometric response of one of the inner junctions is plotted in Fig. 4(a) for different values of I_{bias}. A responsivity up to approximately 0.6 mV/K was obtained for a 20-pA bias (see Fig. 4(b)).

The wider tunnel contacts fabricated at the end of the NWs were used to demonstrate the local refrigeration of an individual NW. Electronic cooling in the SI(NW)IS device relies on the presence of a forbidden gap for the quasiparticles in the superconductors, which induces the equivalent of evaporative cooling on the electrons in the NW (see sketch in Fig. 4(c)). Up to a bias on the order of Δ, only hot electrons can leave the NW region, effectively cooling the electronic distribution. Two devices called *A* and *B* were tested in such a cooling configuration. The corresponding steady-state temperatures for different bias voltages V_{refr} are plotted in Fig. 4(d). In this case, at a finite V_{refr} bias, we expect that $T_e \neq T_{bath}$ and $T_e(V_{refr})$ can be extracted from the thermometer calibration of Fig. 4(a). The amount of cooling in the NW can be quantified by comparing T_e at $V_{refr} = 0$ (where $T_e = T_{bath}$, as indicated by the reference dashed line) and T_e at a finite bias. The largest cooling was achieved for $|qV_{refr}| \approx \Delta_0$, and heating was obtained for a larger bias, as expected for a single NIS cooler [4]. This behavior is consistent with the non-ideal behavior of current devices, where one of the two cooling contacts is typically too transparent. Once the minimum electron temperatures $T_{e,min}$ were extracted from the $T_e(V_{refr})$ curves, the largest temperature reduction $\delta T_{max} = T_{bath} - T_{e,min}$ of ~10 mK was found to occur at $T_{bath} \approx 250$–350 mK, as shown in Fig. 4(e). The cooling effect remained modest, indicating that our tunnel junction can be effectively used to reduce the electronic temperature in an individual NW. Various non-ideal factors hamper the device performance in the current architecture: (i) The tunnel barrier cools the whole AlMn region, which is wider that the NW (see sketch in Fig. 1(c)); (ii) the barrier opacity is not optimal, and typically one of the two contacts of the refrigerator is too transparent. A possible route for achieving better performance consists of patterning different geometries for the AlMn and Al layers, in order to achieve tunnel junctions that are more controlled and have a smaller area in correspondence with the NW body.

In conclusion, we demonstrated an original technique for the fabrication of superconducting tunnel junctions on InAs-based semiconductor NWs. The junctions were shown to be suitable for low-temperature thermometry, and electronic cooling was demonstrated at the optimal biasing conditions. The relatively small cooling observed in the present devices does not represent a fundamental limitation and can be significantly improved by using an optimized contact geometry. This technology can have a large impact on cryogenic circuits requiring local cooling and can benefit numerous nanoscience fields, including sensing, quantum computation, and quantum in general.

2 Methods

Selenium-doped InAs NWs were grown via chemical beam epitaxy on a InAs 111B substrate. Gold catalyst colloid nanoparticles 40 nm in diameter were dispersed on the substrate, and InAs NWs were grown at 400 °C for 60 min using tertiarybutylarsine (1.5 Torr), trimethylindium (0.6 Torr), and tertiarybutylselenide (0.3 Torr). Then, the growth temperature was increased to 440 °C, and the growth was conducted for another 50 min. The NWs typically had a diameter $d = 90 \pm 10$ nm and a length of ~2.5 µm. Electron-beam lithography was performed using positive poly(methyl methacrylate) (PMMA, AR-P 679.04) with a 20-kV acceleration voltage and a dose of 320 µC/cm^2. The development was performed in a 1:3 solution of an AR 600-56 PMMA developer and isopropanol, and the possible residuals of the resist were removed via plasma O cleaning. Immediately before the evaporation, the samples were immersed in a 48 °C $(NH_4)_2S_x$ solution for 1 min to remove native oxide from the top of the NW for minimizing unwanted scattering in the interface of the contacts. Then, they were immersed for 1 min in water and quickly rinsed in isopropanol before being moved into an ultrahigh-vacuum evaporator with a base vacuum of 10^{-10} Torr. The first 5-nm-thick Ti layer was evaporated at a rate of 1 Å/s to form a sticking layer. A 50-nm-thick $Al_{0.98}Mn_{0.02}$ layer was then evaporated on top of the Ti at 1.5 Å/s. Subsequently, the samples were reinserted into the loading chamber for oxidation in O_2 at 0.2–0.4 Torr for 5 min. The final evaporation was then completed again in the main chamber to obtain a 50-nm-thick pure Al layer at 1.5 Å/s. Liftoff was performed in 50 °C acetone before the samples were finally rinsed with isopropanol. For measurement, the samples were bonded with Al wires to a 24-legged sample holder; thus, six NW devices were measured with a single bonding. All the measurements

were performed in a cryo-free ^{3}He/^{4}He dilution refrigerator with a base temperature of 30 mK. First, the junctions were characterized by applying a bias voltage using a direct-current voltage source and measuring the current flowing through a room-temperature current preamplifier with a varying cryostat temperature and off-plane magnetic field. The filtering included two low-pass RC filters and two LC π-filters anchored at the base temperature, as well as an additional LC π-filter stage at room temperature.

A theoretical comparison for the measured data was performed using BSC theory for SINIS tunnel junctions, assuming the quasi-equilibrium of the electrons in the normal metal. The current I flowing through a SINIS junction with respect to the bias voltage V can be expressed as

$$I(V) = \frac{1}{eR_N}\int_{-\infty}^{\infty} n_S(E)\left[f_N\left(E - e\frac{V}{2}, T_e\right) - f_N\left(E + e\frac{V}{2}, T_e\right)\right] dE, \quad (1)$$

where R_N is the total normal-state resistance of the junction, and

$$n_S(E) = \left|\mathrm{Re}\left[\frac{E + i\gamma\Delta}{\sqrt{(E+i\gamma\Delta)^2 - \Delta^2}}\right]\right| \quad (2)$$

is the normalized density of states in the superconductor [4], with the Dynes parameter γ indicating the life-time broadening of the quasi-particles or the photon-assisted tunneling leading to the non-ideal behavior of the superconductor [40]. The temperature dependence of $\Delta(T)$ was considered as well. In the above expression

$$f_N(E, T_e) = \frac{1}{e^{E/k_B T_e} + 1} \quad (3)$$

is the Fermi–Dirac distribution of the normal metal. The conductance was obtained by differentiating Eq. (1).

Acknowledgements

S. R., V. Z., L. S, D. E., and M. R. acknowledge the financial support by CNR, through the bilateral projects with RFBR (Russia), and by Scuola Normale Superiore. The work of E. S. is funded by the Marie Curie Individual Fellowship MSCAIFEF-ST No. 660532-SuperMag. F. G, N. L., and A. F. acknowledge the financial support of the European Research Council under the European Union's Seventh Framework Program (No. FP7/2007-2013)/ERC Grant agreement (No. 615187-COMANCHE) and MIURFIRB2013–Project Coca (No. RBFR1379UX). I. M. acknowledges funding by the Academy of Finland grant No. 260880.